Published in final edited form as:
Phys Med Biol. 2010 December 7; 55(23): 7067–7080. doi:10.1088/0031-9155/55/23/S08.

Predicted risks of second malignant neoplasm incidence and mortality due to secondary neutrons in a girl and boy receiving proton craniospinal irradiation

Phillip J Taddei[1,3], **Anita Mahajan**[2], **Dragan Mirkovic**[1], **Rui Zhang**[1], **Annelise Giebeler**[1], **David Kornguth**[2], **Mark Harvey**[1], **Shiao Woo**[2], and **Wayne D Newhauser**[1]

[1] Department of Radiation Physics, The University of Texas M D Anderson Cancer Center, 1515 Holcombe Blvd, Houston, TX 77030, USA

[2] Department of Radiation Oncology, The University of Texas M D Anderson Cancer Center, 1515 Holcombe Blvd, Houston, TX 77030, USA

Abstract

The purpose of this study was to compare the predicted risks of second malignant neoplasm (SMN) incidence and mortality from secondary neutrons for a 9-year-old girl and a 10-year-old boy who received proton craniospinal irradiation (CSI). SMN incidence and mortality from neutrons were predicted from equivalent doses to radiosensitive organs for cranial, spinal and intracranial boost fields. Therapeutic proton absorbed dose and equivalent dose from neutrons were calculated using Monte Carlo simulations. Risks of SMN incidence and mortality in most organs and tissues were predicted by applying risks models from the National Research Council of the National Academies to the equivalent dose from neutrons; for non-melanoma skin cancer, risk models from the International Commission on Radiological Protection were applied. The lifetime absolute risks of SMN incidence due to neutrons were 14.8% and 8.5%, for the girl and boy, respectively. The risks of a fatal SMN were 5.3% and 3.4% for the girl and boy, respectively. The girl had a greater risk for any SMN except colon and liver cancers, indicating that the girl's higher risks were not attributable solely to greater susceptibility to breast cancer. Lung cancer predominated the risk of SMN mortality for both patients. This study suggests that the risks of SMN incidence and mortality from neutrons may be greater for girls than for boys treated with proton CSI.

1. Introduction

In the pursuit of reducing side effects in non-target tissues, proton radiotherapy is a particularly suitable treatment modality for some treatment sites due to its sharp distal fall-off in dose, which reduces the integral dose to the patient (Kirsch and Tarbell 2004, St Clair *et al* 2004, Yuh *et al* 2004). Normal tissue sparing is paramount for children because of their susceptibility to radiation-induced late effects, with carcinogenesis of greatest concern. Three main factors make children more vulnerable to radiogenic late effects than adults: (1) children's developing tissues and organs have higher radiosensitivity; (2) children's smaller statures put their non-target organs in closer proximity to the therapeutic fields and (3) many children have longer expected survival times than adults undergoing similar therapies.

[3]Author to whom any correspondence should be addressed. ptaddei@mdanderson.org.

(Some figures in this article are in colour only in the electronic version)

The Childhood Cancer Survivor Study (CCSS) has provided valuable information on the occurrence of late effects of cancer treatments in children. For example, Meadows *et al* (2009) found a 9.3% incidence of second malignant neoplasms (SMNs), excluding non-melanoma skin cancer (NMSC), and a 6.9% incidence of NMSC, at 30 years after diagnosis of the first cancer, and the values are increasing with the number of years of follow-up. Exposure to radiation was cited as the most frequent predisposing factor for subsequent neoplasms. Armstrong *et al* (2009) reported that children in the CCSS who were diagnosed with primitive neuroectodermal tumor were 23.4 (95% confidence interval, 12.4–40.0) times more likely to die of a non-recurrent subsequent malignancy than children in the general population. However, these CCSS enrolled survivors were diagnosed between 1970 and 1986; children who have received advanced radiotherapies, for example intensity-modulated photon therapy and proton therapy, were not included. Thus, until long-term outcome data for patients receiving these advanced treatments are available, predictions of late effects must be calculated using accurate dose reconstructions and risk models.

Several studies have reported on the stray (i.e. non-therapeutic) radiation exposures to patients receiving passively scattered proton therapy (PSPT), in which the equivalent dose from stray radiation per therapeutic absorbed dose was calculated or measured (Schneider *et al* 2002, Fontenot *et al* 2008, Zacharatou Jarlskog *et al* 2008, Taddei *et al* 2009a, Wroe *et al* 2009). Among the many particles that contribute to this stray dose, neutrons are of primary concern (Agosteo *et al* 1998) because the relative biological effectiveness (RBE) of neutrons for carcinogenesis is generally greater than for other particles and is poorly understood.

In previous studies, estimates of risk of SMNs were based on the equivalent dose in radiosensitive organs and tissues. In treatment planning studies, Miralbell *et al* (2002) and Mu *et al* (2005) compared the risks of SMNs after proton and intensity-modulated photon irradiation of the spinal axis in children (age 3 years for Miralbell *et al* and ages 6–11 years for Mu *et al*). In both studies, proton therapy conferred one-eighth of the risk of SMN incidence of photon therapy, although the contributions to risk from neutrons were neglected. In a subsequent study, Newhauser *et al* (2009a) supplemented the analysis from Miralbell *et al* to include neutron radiation and added a cranial field to better reflect clinical practice. Newhauser *et al* found that neutrons increased the predicted risk of an SMN slightly but that proton therapy still carried a lower risk than photon therapy. The results from Miralbell *et al* and Newhauser *et al* were based on one patient each, and the dosimetric uncertainties were large and difficult to estimate. Taddei *et al* (2009a) estimated the risk of developing a fatal SMN from neutrons for boys who receive proton craniospinal irradiation (CSI); the spinal fields predominated this risk while the cranial and intracranial boost fields played a comparatively small role. However, this study was based on one male patient, and predicted SMN incidence and mortality are known to depend strongly on sex (Armstrong *et al* 2007). Differences between predicted risks following proton CSI for females versus males remained to be determined.

The aim of this study was to compare the risks of SMN incidence and mortality from neutrons for two pre-pubescent children, a girl and a boy of similar stature, who received proton CSI for cancers of the central nervous system. The predicted risks were based on Monte Carlo (MC) calculations of equivalent dose from secondary neutrons for a complete proton CSI, including intracranial boost fields, and risk models from the literature. We used MC simulations to calculate separately the absorbed dose from primary (therapeutic) protons, the equivalent dose from neutrons originating in the treatment unit, or ‘external neutrons,’ and the equivalent dose from neutrons originating within the patient, or ‘internal neutrons,’ for PSPT.

2. Methods and materials

2.1. Proton treatment technique

Proton radiotherapy plans were created as previously described (Newhauser *et al* 2007) using a commercial treatment planning system (TPS) (Eclipse Proton; Varian Medical Systems, Inc., Palo Alto, CA) and kilovoltage computed tomography (CT) images for a 9 year old girl with medulloblastoma and a 10 year old boy with supratentorial primitive neuroectodermal tumor. Organ and tissue structures were contoured using the TPS. The RBE of therapeutic protons throughout the treatment volume was taken as 1.1 (ICRU 2007). Each field had a specific clinical target volume (CTV). The CTVs for the cranial and spinal fields were abutted to deliver a uniform dose to the entire craniospinal axis. The boost fields shared a common CTV, which was the gross tumor volume in the brain with an additional margin. The cranial fields also shared a common CTV. For this study, the treatment plans for both children specified 21.3 Gy proton absorbed dose to the craniospinal axis and an additional 27.8 Gy proton absorbed dose to the boost CTV. Field characteristics for the two patients are listed in table 1. For fields that shared a common CTV, the prescribed dose was divided evenly between the fields. Snout sizes and further details of other treatment parameters were described previously (Taddei *et al* 2009a). The plan was exported from the TPS for the MC simulation.

2.2. Treatment unit and patient modeling

Simulations were performed with the Monte Carlo Proton Radiotherapy Treatment Planning system (Newhauser *et al* 2007, 2008b), which used the Monte Carlo N-Particle eXtended code version 2.6b (Pelowitz 2008) with parallel processing (2.6 GHz, 64-bit processors; AMD Opteron; Advanced Micro Devices, Inc., Sunnyvale, CA) as a radiation dose calculation engine. Each component of the treatment unit was modeled in detail (Newhauser *et al* 2007, Zheng *et al* 2008). The planning CT images extended from the top of the head to the thighs and ankles for the girl and boy, respectively. The CT number in each voxel was converted to a mass density and a material composition in the geometric model using a machine-specific calibration curve (Newhauser *et al* 2008a). In the MC code, lattices of 1.3×10^6 and 2.0×10^6 voxels were used to represent the girl and boy, respectively. A detailed description of these methods was provided elsewhere (Taddei *et al* 2009a).

2.3. Dosimetric calculations

The absorbed dose in each voxel, D_v, was calculated in separate simulations both for each treatment field and for each radiation type—therapeutic protons, external neutrons and internal neutrons. The results of the MC simulations were converted to absorbed dose per source particle, D_v/sp (in Gy sp^{-1}). Because each voxel had the same volume, the mass-averaged absorbed dose, D_T, for each organ or tissue, T, was calculated as the density-weighted average absorbed dose over all the voxels within that organ or tissue according to

$$D_T = \frac{\sum_{v \text{in} T} D_v \rho_v}{\sum_{v \text{in} T} \rho_v}, \quad (1)$$

where ρ_v is the mass density of voxel v. D_T was calculated for each radiation type in each contoured organ and tissue, including the CTV of each therapeutic field. The D_T per source particle from therapeutic protons in the CTV, D_{CTV}/sp, was used to normalize the values of D_v per therapeutic Gy as follows: D_{CTV}/sp was calculated for each treatment field. D_v/sp for each radiation type was then divided by D_{CTV}/sp separately for each treatment field, resulting in D_v and D_T in mGy Gy^{-1} for each radiation type and treatment field.

Equivalent dose from neutrons in organ or tissue T, H_T, was calculated as the product of the mean neutron radiation weighting factor, $\overline{w_R}$, and the neutron D_T:

$$H_T = \overline{w_R} D_T. \tag{2}$$

H_T values were calculated separately for internal and external neutrons for each treatment field. Values of $\overline{w_R}$ were determined separately for each field as

$$\overline{w_R} = \int \varphi(E_n) w_R(E_n) \mathrm{d}E_n, \tag{3}$$

where $\varphi(E_n)$ was the neutron spectral fluence. The energy-dependent expression of the neutron radiation weighting factor, $w_R(E_n)$, followed the recommended procedure from International Commission on Radiological Protection (ICRP) *Publication 92* (ICRP 2003):

$$w_R(E_n) = 2.5 \left\{ 2 - \mathrm{e}^{-4E_n} + 6\,\mathrm{e}^{-\frac{1}{4}(\ln E_n)^2} + \mathrm{e}^{-\frac{1}{2}\left[\ln\left(\frac{E_n}{30}\right)\right]^2} \right\}, \tag{4}$$

where E_n was the neutron energy in MeV. For internal neutrons, the values of $\overline{w_R}$ were taken from Newhauser *et al* (2009a) in which organ-specific $\overline{w_R}$ values were estimated using equations (3) and (4) above and the neutron spectral fluence values were tallied within the internal organs of an anthropomorphic phantom receiving proton CSI. They found that $\overline{w_R}$ values averaged over all organs were 9.7 for the lower spinal field, 9.4 for the upper spinal field and 7.9 for the cranial field. For external neutrons, we calculated $\overline{w_R}$ in a similar manner in this study except that $\varphi(E_n)$ was taken as the spatially averaged neutron spectral fluence incident upon the voxelized phantom. H_T was also calculated per therapeutic absorbed dose to the CTV, H_T/D_{CTV}, in units of mSv Gy^{-1}.

2.4. Effective dose from neutrons

Effective dose is a radiological protection quantity that is useful for quantifying and comparing various radiation exposures. Following the recommendations in *ICRP Publication 92* (ICRP 2003), the effective dose from neutrons, E, was calculated as the sum over all specified organs and tissues, T,

$$E = \sum_T (w_T H_T), \tag{5}$$

where w_T is the tissue weighting factor and H_T is the equivalent dose in an organ or tissue from neutrons. The w_T values (table 2) were taken directly from *ICRP Publication 60* (ICRP 1991) and take into account the differences in the radiosensitivity of various organs and tissues. The w_T for the remainder was applied to the average H_T value of all voxels in the phantom. E was also calculated per therapeutic absorbed dose to the CTV, E/D_{CTV}, in units of mSv Gy^{-1}.

2.5. Risks of SMN incidence and mortality

Lifetime absolute risks of SMN incidence, I_T, and mortality, M_T, attributable to neutron exposures were estimated for specific cancer sites that correspond to T. Age-, sex- and organ-specific risk coefficients were applied to the values of H_T as follows:

$$I_T = \left(\frac{I_T}{H_T}\right)_{\text{BEIRVII}} \cdot H_T \qquad M_T = \left(\frac{M_T}{H_T}\right)_{\text{BEIRVII}} \cdot H_T, \tag{6}$$

where risk coefficients for incidence, I_T/H_T, and mortality, M_T/H_T, were taken directly from the *BEIR VII Report* (NRCNAS 2006) (see table 2). These risk coefficients were already adjusted by a dose and dose rate effectiveness factor (DDREF) of 1.5, except for leukemia, which was based on a linear-quadratic model. The leukemia risk coefficients for incidence and mortality were applied to the H_T value for the red bone marrow, and the 'other' risk coefficients for incidence and mortality were applied to the average H_T value of all voxels in the phantom.

A slightly different procedure was followed to predict the incidence of NMSC. Although NMSC is considered radiogenic, it was excluded from the selected risk model in the *BEIR VII Report* because NMSC exhibits 'exceptionally strong age dependences that do not seem to be typical of cancers of other sites' (NRCNAS 2006, p 298). Like thyroid cancer, NMSC is rarely fatal. However, the incidence of skin cancer is large in survivors of childhood cancer (Meadows *et al* 2009) and therefore should be taken into account in predictions of SMN incidence. Therefore, to estimate the risk of NMSC for these two patients, we applied the risk model recommended in *ICRP Publication 60* (ICRP 1991):

$$I_{\text{skin}} = \left(\frac{M_{\text{skin}}}{H_{\text{skin}}}\right)_{\text{ICRP}} \cdot \frac{1}{L_{\text{skin}}} \cdot \frac{1}{\text{DDREF}} \cdot H_{\text{skin}} \qquad M_{\text{skin}} = I_{\text{skin}} \cdot L_{\text{skin}}, \tag{7}$$

where L_{skin} is the organ-specific lethality factor for NMSC. The $M_{\text{skin}}/H_{\text{skin}}$ and L_{skin} values for NMSC were 0.02% Sv^{-1} and 0.002, respectively. Because the equivalent doses to organs and tissues from neutrons are less than 0.1 Sv per fraction, I_{skin} was reduced by a DDREF of 2 (ICRP 1991).

2.6. Statistical uncertainty in dosimetric quantities and risk

We tracked 25 billion source protons and associated secondary protons and neutrons in each simulation to minimize statistical fluctuations in D_T. The statistical uncertainties, σ, in D_T, H_T, E, and risk were estimated considering only statistical fluctuations reported by the MC code for D_v and are reported at the 68% confidence interval. We excluded the uncertainties in the risk models and in $\overline{w_R}$ (Newhauser *et al* 2009a, 2009b) (see section 4).

3. Results

3.1. Equivalent dose from neutrons

The distributions of absorbed dose from therapeutic protons and equivalent dose from neutrons in the girl's anatomy are shown in figure 1. The therapeutic proton dose distribution was highly localized to the brain and spine while dose from secondary neutrons pervaded the entire body. The dose distributions for the boy (see Taddei *et al* 2009a for the boy's neutron dose distribution) were qualitatively similar to those for the girl.

Table 3 lists the values of H_T/D_{CTV} in various organs and tissues for each treatment field. The H_T/D_{CTV} values, which include contributions from external and internal neutrons, strongly depended on the locations of T and the treatment field; they ranged from 0.44 mSv Gy^{-1} to 12.3 mSv Gy^{-1} for the girl and 0.35 mSv Gy^{-1} to 14.0 mSv Gy^{-1} for the boy. In most organs and tissues, the largest values generally were associated with the spinal fields;

for the bone surface, skin and remainder (i.e. whole body), however, the largest values were associated with the cranial fields.

The total neutron equivalent dose values from all fields, H_T, are also listed in table 3 for each organ or tissue. For the red bone marrow, gonads and bladder, the girl's H_T values were more than 20% larger than the boy's; for the thyroid, lungs, and esophagus, the boy's H_T was more than 20% larger than the girl's. For both patients, the esophagus, thyroid, lungs and bone surface had the largest H_T values and the gonads had the smallest H_T values. For the most radiosensitive organs, the boost fields made very little contribution to H_T because the boost volume was small and was located far away from the organ. The values of σ in H_T were less than 2.6% for each organ.

For each patient, the $\overline{w_R}$ values associated with each field were calculated in separate simulations for external neutrons. These values were similar for the girl (range, 8.8–9.6) and boy (9.1–10.0).

3.2. Effective dose from neutrons

The values of E from neutrons were similar for the girl and boy. For the entire treatment, E was 428 mSv (σ_E/E = 0.3%) for the girl and 418 mSv (σ_E/E = 0.2%) for the boy. For both patients, the two spinal fields contributed the most to E (291 mSv total for the girl and 302 mSv total for the boy), whereas the boost fields contributed relatively little (30 mSv total for the girl and 22 mSv total for the boy). For the entire set of treatment fields, external neutrons contributed 326 mSv and 344 mSv to E for the girl and boy, respectively, and internal neutrons contributed 102 mSv and 74 mSv, respectively. For both children, the organs that contributed the most to E was the lungs (66 mSv for the girl and 61 mSv for the boy). E/D_{CTV} values for the CSI fields in particular were 13.0 mSv Gy^{-1} for the girl and 12.9 mSv Gy^{-1} for the boy. Thus, the relative contributions from each type of field to E and those from each source of neutrons to E were similar for the girl and boy.

3.3. Risk of SMN incidence and mortality

The predicted lifetime risks of SMN incidence from neutrons were 14.8% for the girl and 8.5% for the boy, which include a 2.7% lifetime risk of NMSC for the girl and a 2.3% lifetime risk of NMSC for the boy. The difference was predominated by sex-specific differences in the risk coefficients; differences in H_T and $\overline{w_R}$ values were of lesser importance. The predictions of site-specific cancer incidence for each patient are shown in figure 2. For each cancer site, the risks were generally higher for the girl than for the boy, with the exceptions of colon and liver cancers. The girl's predicted SMN incidence was predominated by the risks of breast, skin, lung and thyroid cancers; the boy's predicted SMN incidence was predominated by the risks of skin, lung and colon cancers.

The predicted lifetime risks of SMN mortality from neutrons were 5.3% for the girl and 3.4% for the boy. Like the risk of SMN incidence, the risk of SMN mortality was higher for the girl than for the boy because the risk coefficients were larger for the girl. The predicted risks of fatal SMNs at each cancer site are shown in figure 3 for both patients. The M_T values were generally higher for the girl than for the boy, with the exceptions of death due to cancers of the colon and liver. Lung cancer predominated the risk of mortality for both children, followed by breast cancer risk in the girl and colon cancer risk in the boy.

The results for the girl and boy are summarized in table 4, including a list of organs and tissues with I_T greater than 0.8% or M_T greater than 0.4%.

4. Discussion

Our results suggest that, for survivors of childhood cancer, girls receiving CSI by means of PSPT may have almost twice the risks of SMN incidence and mortality from neutrons than boys do over the course of their lifetimes. In the treatments simulated here, the effective doses from neutrons for the two patients were similar (~420 mSv, or the equivalent of about 20 whole-body CT scans), yet our results revealed that the girl had higher predicted risks than the boy for all SMNs, except those in the liver and colon. Thus, the differences in risks could not be attributed solely to a difference in risks associated with breast cancer. Rather, the higher predicted risks for the girl than the boy were mainly attributable to the larger risk coefficients for most organs and tissues in girls than those in boys while the dosimetric differences between the sexes were less important. The clinical implication of this finding is that, in cases where the risks of SMNs are of concern, the patient's sex is an important factor.

The sex-related differences in risk predicted in this study agree reasonably well with some epidemiologic studies in the literature. In a review article, Armstrong *et al* (2007) highlighted studies that documented a difference between the sexes in the probability of late effects, including SMNs. Most studies in the review indicated a greater risk for females than males. For example, in the CCSS cohort, Neglia *et al* (2001) reported a relative risk of 1.64 ($p < 0.001$) for the occurrence of any SMN in females versus males; however, no increase in risk was observed for leukemia, central nervous system tumors, bone cancers, soft-tissue sarcomas and thyroid cancers. It is noteworthy that one study (Devarhally *et al* 2003) reported larger risks for males than females who received local (e.g. intracranial) or regional (e.g. CSI) treatments, but the true radiation-related risk differential may have been masked by confounding factors. In addition, studies that aggregated radiotherapy for multiple CNS cancers are of limited relevance to survivors who received CSI because of the vastly different SMN risks following regional and local irradiation (Newhauser *et al* 2009a, Taddei *et al* 2009a). Together, this evidence strongly suggests that risk projections for patients who receive CSI should take into account sex, age at exposure, treatment technique and anatomical site.

Few other studies have been performed to predict the risk of SMN from secondary neutrons in patients who have received PSPT, and fewer still examined factors contributing to differences in risk. In a study comparing proton therapy with photon therapy, Newhauser *et al* (2009a) predicted the absolute lifetime risk of second cancer incidence due to the stray radiation of 1.5% for a 3 year old boy following a 36 Gy CSI treatment. Their value is one-fifth of the risk of SMN incidence estimated for the 9 year old boy in the present study for two reasons. First, the effective dose from stray radiation was 55% less for the boy in the earlier study (187 mSv) than for the boy in our study (418 mSv) because Newhauser *et al* used an adult-sized phantom to represent the patient, meaning that the organs were farther away from the therapeutic fields and because the air gap between the patient and the treatment unit was larger; both factors likely reduced their calculated neutron exposures (Taddei *et al* 2008, 2009a, 2009b, Zheng *et al* 2008, Brenner *et al* 2009). Second, Newhauser *et al* applied risk models from *ICRP Publication 60* (ICRP 1991), whereas we used models from the *BEIR VII Report* (NRCNAS 2006) for all organs except skin. The selection of risk model can strongly influence predictions of absolute risk (Fontenot *et al* 2009). It is important that the organs at greatest risk for SMN incidence for the boy in our study (skin, thyroid, colon and lungs) were also included among the major organs at risk for SMN in the study by Newhauser *et al.*

Zacharatou Jarlskog and Paganetti (2008) estimated the neutron-induced risk of SMN incidence following PSPT of localized brain lesions for several therapeutic intracranial

fields and for patients of various ages. Their methods were similar to those for the boost fields in this study, except that they approximated patient treatments using phantoms from the literature and circular intracranial fields. Their estimates of lifetime risk of SMN incidence from secondary neutrons for 8 year old girls ranged from 1% to 3%, which generally agrees with those from the boost fields in our study if we scale our results to match their 70 Gy therapeutic dose and neglect the contribution from NMSC. Like us, they also estimated the proportion of risk attributable to neutrons emitted from the treatment unit at 80%. Recently, Athar and Paganetti (2009) extended the study by Zacharatou Jarlskog and Paganetti to include spinal fields. However, it is difficult to directly compare their findings and ours because of the differences in the spinal treatment field characteristics (they used simplistic circular fields, whereas we used realistic, patient-specific rectangular fields). Together, those studies and ours showed that, for children receiving proton CSI, predicted neutron doses and risks of SMN incidence and mortality depend strongly on the patient's age at exposure, stature, sex and the anatomical location of the treatment fields.

The present study has several strengths. We compared the risks of SMN incidence and mortality in a boy and a girl receiving proton CSI while controlling for age at exposure, attained age, patient size and anatomical treatment site. By using patient-specific voxelized phantoms, implementing field-specific models for each major component of the PSPT treatment unit, simulating all the treatment fields that the patients would receive, and applying a cancer-site-specific risk model, we achieved an enhanced level of realism and completeness for CSI patients. Finally, we maintained our ability to use large-scale parallel computing techniques, resulting in small statistical uncertainties in the calculated equivalent dose values.

The largest uncertainty in our risk predictions lies in the risk coefficients. The uncertainties in risk when these coefficients are applied to patients are difficult to estimate because the coefficients are based on data from a healthy population. Furthermore, we used $\overline{w_R}$ to weight the absorbed dose from neutrons, even though $\overline{w_R}$ is a radiological protection quantity and may underestimate or overestimate the true RBE of neutrons for carcinogenesis. However, these limitations are not serious for this study because uncertainties related to the risk coefficients and $\overline{w_R}$ values were lessened by holding all other major confounding factors constant and by comparing differences in risk only between the two sexes. The impact of the uncertainty in the risk models and $\overline{w_R}$ values on SMN risk estimates for patients undergoing proton CSI were addressed previously (Newhauser *et al* 2009a).

This study had two limitations related to the dosimetric calculations. First, the air gap between the treatment unit and the patient was slightly larger for the girl than for the boy. Previous studies (Fontenot *et al* 2008, Zheng *et al* 2008, Taddei *et al* 2009a) demonstrated a moderate inverse relationship between secondary neutron dose and air gap. However, although the girl's larger air gap may have decreased the exposure to secondary neutrons, her effective dose was similar to the boy's. A second potential source of systematic bias in dose was that the girl's legs were not included in the voxelized phantom representing her, whereas the boy's were. Because the legs were farther from the fields than the rest of the body, the equivalent dose to the red bone marrow, skin and entire body in the legs was less than those of the rest of the body. Thus, the absence of this lower-dose region for the girl may have resulted in a slight overestimation in equivalent dose to the red bone marrow, the skin and the remainder because the contours for these organs and tissues were approximated as being above the lowest CT slice. Because the dosimetric impact of these limitations was small, they are not serious and do not change our conclusions.

In conclusion, we found that the predicted risks of SMN incidence and mortality due to neutrons following proton CSI were greater for a girl than a boy of similar age and stature.

This finding highlights the importance of sex-specific risk estimation for children receiving CSI and suggests that sex-specific risk estimates may also be important for treatments of other anatomical sites.

Acknowledgments

This work was supported in part by the National Cancer Institute (awards 1R01CA131463-01A1 and F32CA128340-01A1), by Northern Illinois University through a subcontract of Department of Defense (award W81XWH-08-1-0205), and by the Fogarty International Center (award K01TW008409). The content is solely the responsibility of the authors and does not necessarily represent the official views of the sponsors. We acknowledge Kathryn B Carnes for her assistance in preparing this manuscript and Rebecca Howell, Sarah Scarboro, Uwe Titt, Laura Rechner, Pablo Yepes, and Sharmalee Randeniya for their helpful scientific suggestions.

References

Agosteo S, Birattari C, Caravaggio M, Silari M, Tosi G. Secondary neutron and photon dose in proton therapy. Radiother Oncol 1998;48:293–305. [PubMed: 9925249]

Armstrong GT, Sklar CA, Hudson MM, Robison LL. Long-term health status among survivors of childhood cancer: does sex matter? J Clin Oncol 2007;25:4477–89. [PubMed: 17906209]

Armstrong GT, Liu Q, Yasui Y, Neglia JP, Leisenring W, Robison LL, Mertens AC. Late mortality among 5-year survivors of childhood cancer: a summary from the Childhood Cancer Survivor Study. J Clin Oncol 2009;27:2328–38. [PubMed: 19332714]

Athar BS, Paganetti H. Neutron equivalent doses and associated lifetime cancer incidence risks for head & neck and spinal proton therapy. Phys Med Biol 2009;54:4907–26. [PubMed: 19641238]

Brenner DJ, Elliston CD, Hall EJ, Paganetti H. Reduction of the secondary neutron dose in passively scattered proton radiotherapy, using an optimized pre-collimator/collimator. Phys Med Biol 2009;54:6065–78. [PubMed: 19779218]

Devarhally SR, Severson RK, Chuba P, Thomas R, Bhambhani K, Hamre MR. Second malignant neoplasms after primary central nervous system malignancies of childhood and adolescence. Pediatr Hematol Oncol 2003;20:617–25. [PubMed: 14578032]

Fontenot JD, Lee AK, Newhauser WD. Risk of secondary malignant neoplasms from proton therapy and intensity-modulated x-ray therapy for early-stage prostate cancer. Int J Radiat Oncol Biol Phys 2009;74:616–22. [PubMed: 19427561]

Fontenot JD, Taddei P, Zheng Y, Mirkovic D, Jordan T, Newhauser WD. Equivalent dose and effective dose from stray radiation during passively scattered proton radiotherapy for prostate cancer. Phys Med Biol 2008;53:1677–88. [PubMed: 18367796]

ICRP (International Commission on Radiological Protection). Recommendations of the International Commission on Radiological Protection: ICRP Publication 60. Ann ICRP 1991;21(1–3)

ICRP (International Commission on Radiological Protection). Relative biological effectiveness (RBE), quality factor (Q), and radiation weighting factor (w_R): ICRP Publication 92. Ann ICRP 2003;33(4)

ICRU (International Commission on Radiation Units and Measurements). ICRU Report. Vol. 78. Oxford: Oxford University Press; 2007. Prescribing, recording, and reporting proton-beam therapy.

Kirsch DG, Tarbell NJ. New technologies in radiation therapy for pediatric brain tumors: the rationale for proton radiation therapy. Pediatr Blood Cancer 2004;42:461–4. [PubMed: 15049021]

Meadows AT, Friedman DL, Neglia JP, Mertens AC, Donaldson SS, Stovall M, Hammond S, Yasui Y, Inskip PD. Second neoplasms in survivors of childhood cancer: findings from the Childhood Cancer Survivor Study cohort. J Clin Oncol 2009;27:2356–62. [PubMed: 19255307]

Miralbell R, Lomax A, Cella L, Schneider U. Potential reduction of the incidence of radiation-induced second cancers by using proton beams in the treatment of pediatric tumors. Int J Radiat Oncol Biol Phys 2002;54:824–9. [PubMed: 12377335]

Mu X, Bjork-Eriksson T, Nill S, Oelfke U, Johansson KA, Gagliardi G, Johansson L, Karlsson M, Zackrisson DB. Does electron and proton therapy reduce the risk of radiation induced cancer after

spinal irradiation for childhood medulloblastoma? A comparative treatment planning study. Acta Oncol 2005;44:554–62. [PubMed: 16165914]

Neglia JP, Friedman DL, Yasui Y, Mertens AC, Hammond S, Stovall M, Donaldson SS, Meadows AT, Robison LL. Second malignant neoplasms in five-year survivors of childhood cancer: childhood cancer survivor study. J Natl Cancer Inst 2001;93:618–29. [PubMed: 11309438]

Newhauser W, Fontenot J, Zheng Y, Polf J, Titt U, Koch N, Zhang X, Mohan R. Monte Carlo simulations for configuring and testing an analytical proton dose-calculation algorithm. Phys Med Biol 2007;52:4569–84. [PubMed: 17634651]

Newhauser WD, et al. The risk of developing a second cancer after receiving craniospinal proton irradiation. Phys Med Biol 2009a;54:2277–91. [PubMed: 19305036]

Newhauser WD, et al. Contemporary proton therapy systems adequately protect patients from exposure to stray radiation. AIP Conf Proc 2009b;1099:450–5. [PubMed: 20844607]

Newhauser WD, Giebeler A, Langen KM, Mirkovic D, Mohan R. Can megavoltage computed tomography reduce proton range uncertainties in treatment plans for patients with large metal implants? Phys Med Biol 2008a;53:2327–44. [PubMed: 18421122]

Newhauser WD, Zheng Y, Taddei PJ, Mirkovic D, Fontenot JD, Giebeler A, Zhang R, Titt U, Mohan R. Monte Carlo proton radiation therapy planning calculations. Trans Am Nucl Soc 2008b;99:63–4.

NRCNAS (National Research Council of the National Academy of Sciences). Health Risks From Exposure to Low Levels of Ionizing Radiation: BEIR VII—Phase 2. Washington, DC: National Academies Press; 2006.

Pelowitz, DB. MCNPX™ User's Manual. Los Alamos, NM: Los Alamos National Laboratory; 2008. Version 2.6.0

Schneider U, Agosteo S, Pedroni E, Besserer J. Secondary neutron dose during proton therapy using spot scanning. Int J Radiat Oncol Biol Phys 2002;53:244–51. [PubMed: 12007965]

St Clair WH, Adams JA, Bues M, Fullerton BC, La Shell S, Kooy HM, Loeffler JS, Tarbell NJ. Advantage of protons compared to conventional x-ray or IMRT in the treatment of a pediatric patient with medulloblastoma. Int J Radiat Oncol Biol Phys 2004;58:727–34. [PubMed: 14967427]

Taddei PJ, Fontenot JD, Zheng Y, Mirkovic D, Lee AK, Titt U, Newhauser WD. Reducing stray radiation dose to patients receiving passively scattered proton radiotherapy for prostate cancer. Phys Med Biol 2008;53:2131–47. [PubMed: 18369278]

Taddei PJ, Mirkovic D, Fontenot JD, Giebeler A, Zheng Y, Kornguth D, Mohan R, Newhauser WD. Stray radiation dose and second cancer risk for a pediatric patient receiving craniospinal irradiation with proton beams. Phys Med Biol 2009a;54:2259–75. [PubMed: 19305045]

Taddei PJ, Mirkovic D, Fontenot JD, Giebeler A, Zheng Y, Titt U, Woo S, Newhauser WD. Reducing stray radiation dose for a pediatric patient receiving proton craniospinal irradiation. Nucl Technol 2009b;168:108–12. [PubMed: 20865143]

Wroe A, Clasie B, Kooy H, Flanz J, Schulte R, Rosenfeld A. Out-of-field dose equivalents delivered by passively scattered therapeutic proton beams for clinically relevant field configurations. Int J Radiat Oncol Biol Phys 2009;73:306–13. [PubMed: 19100924]

Yuh GE, Loredo LN, Yonemoto LT, Bush DA, Shahnazi K, Preston W, Slater JM, Slater JD. Reducing toxicity from craniospinal irradiation: using proton beams to treat medulloblastoma in young children. Cancer J 2004;10:386–90. [PubMed: 15701271]

Zacharatou Jarlskog C, Lee C, Bolch WE, Xu XG, Paganetti H. Assessment of organ-specific neutron equivalent doses in proton therapy using computational whole-body age-dependent voxel phantoms. Phys Med Biol 2008;53:693–717. [PubMed: 18199910]

Zacharatou Jarlskog C, Paganetti H. Risk of developing second cancer from neutron dose in proton therapy as a function of field characteristics, organ, and patient age. Int J Radiat Oncol Biol Phys 2008;72:228–35. [PubMed: 18571337]

Zheng Y, Fontenot J, Taddei P, Mirkovic D, Newhauser W. Monte Carlo simulations of neutron spectral fluence, radiation weighting factor and ambient dose equivalent for a passively scattered proton therapy unit. Phys Med Biol 2008;53:187–201. [PubMed: 18182696]

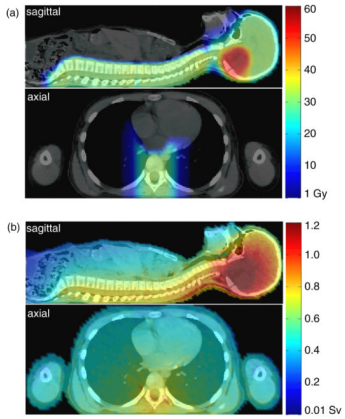

Figure 1.
Midsagittal and axial views of the 9 year old girl revealing (a) the absorbed dose from therapeutic protons and (b) the equivalent dose from neutrons for the entire treatment.

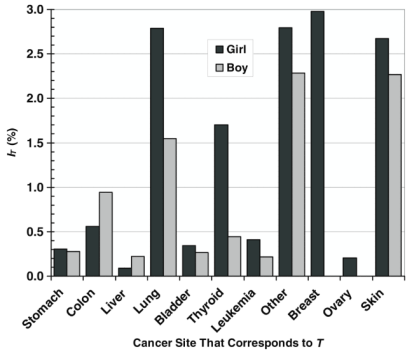

Figure 2.

Lifetime absolute risk of second malignant neoplasm incidence, I_T, from neutrons in specific cancer sites that correspond to organs and tissues, T, for a 9 year old girl and a 10 year old boy after proton craniospinal irradiation.

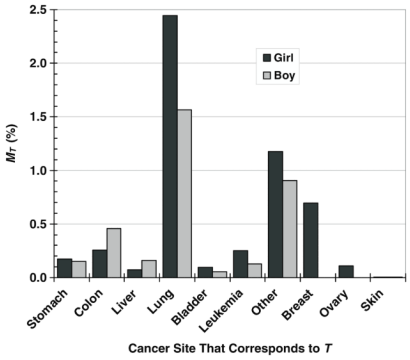

Figure 3.
Lifetime absolute risk of second malignant neoplasm mortality, M_T, due to neutrons in specific cancer sites that correspond to organs and tissues, T, for a 9 year old girl and a 10 year old boy after proton craniospinal irradiation.

Table 1

Treatment technique for all fields in the proton craniospinal irradiations. 'Air gap' refers to the distance between the downstream face of the range compensator and the proximal surface of the patient.

Boy	**LPA**	**UPA**	**RPO**	**LPO**	**LPOB**	**LLB**	
Pre-nozzle proton energy (MeV)	140	140	180	180	160	140	
Range in patient (cm H_2O)	9.4	8.9	16.0	15.9	11.3	9.2	
SOBP width (cm)	7	7	16	16	7	6	
Gantry angle	180°	180°	255°	105°	130°	90°	
Air gap (cm)	10	10	2	2	2	2	
Aperture thickness (cm)	4	4	6	6	4	4	
Collimated field, major axis (cm)	18.4	19.2	19.3	19.8	11.8	11.6	
Collimated field, minor axis (cm)	6.8	6.6	14.3	15.0	5.5	5.4	
Girl	LPA	UPA	RPO	LPO	LPOB	PAB	RPOB
Pre-nozzle proton energy (MeV)	160	160	200	200	160	180	160
Range in patient (cm H_2O)	11.6	11.7	16.5	16.8	12.0	13.5	12.0
SOBP width (cm)	7	6	16	16	8	8	8
Gantry angle	180°	180°	255°	105°	97°	180°	263°
Air gap (cm)	24	24	23	21	23	29	23
Aperture thickness (cm)	4	4	6	6	4	6	4
Collimated field, major axis (cm)	19.8	15.7	15.9	15.9	6.6	7.0	6.3
Collimated field, minor axis (cm)	5.0	4.8	15.2	15.2	6.3	6.3	6.3

Abbreviations: LPA = lower posterior anterior; UPA = upper posterior anterior; RPO = right posterior oblique; LPO = left posterior oblique; LPOB = left posterior oblique boost; LLB = left lateral boost; PAB = posterior anterior boost; RPOB = right posterior oblique boost; SOBP = spread-out Bragg peak.

Table 2

Values applied in this study for tissue weighting factors, w_T, from *ICRP Publication 60* (ICRP 1991) and risk coefficients for incidence, I_T/H_T, and mortality, M_T/H_T, for 10 year olds from Tables 12D-1 and 12D-2 in the *BEIR VII Report* (NRCNAS 2006), listed in terms of absolute risk (in percent) per sievert of equivalent dose.

			Boy		Girl	
Organ or tissue	w_T	**Cancer site**	I_T/H_T (% Sv^{-1})	M_T/H_T (% Sv^{-1})	I_T/H_T (% Sv^{-1})	M_T/H_T (% Sv$^{-1)}$
Gonads	0.20	Ovary			0.7	0.4
Red bone marrow	0.12	Leukemia	1.2	0.7	0.9	0.5
Colon	0.12	Colon	2.4	1.2	1.6	0.7
Lungs	0.12	Lung	2.2	2.2	5.0	4.4
Stomach	0.12	Stomach	0.6	0.3	0.7	0.4
Bladder	0.05	Bladder	1.5	0.3	1.5	0.4
Breasts	0.05	Breast			7.1	1.7
Liver	0.05	Liver	0.4	0.3	0.2	0.2
Esophagus	0.05					
Thyroid	0.05	Thyroid	0.5		2.8	
Skin	0.01	Skin	See the text			
Bone surface	0.01					
Remainder	0.05	Other	5.0	2.0	5.2	2.2

Blank values were taken as zero because they were not included in Tables 12D-1 and 12D-2 in the *BEIR VII Report.* Although specific risk coefficients were also available for cancers of the prostate and uterus, these SMN sites were neglected because the values of equivalent dose in these organs were minimal and the risk coefficients were small.

Table 3

For each organ or tissue, *T*, for the girl and boy, tissue weighting factors, w_T, equivalent dose per therapeutic absorbed dose, H_T/D_{CTV}, for each field, total equivalent dose, H_T, and predicted lifetime SMN incidence, I_T, and predicted lifetime SMN mortality, M_T, for the organs and tissues that correspond to *T*. The data are for both internal and external neutrons. Statistical uncertainties in I_T, M_T and H_T were less than 2.6%. Blank cells represent negligible or not applicable values.

		H_T/D_{CTV} (mSv Gy^{-1})									
Girl Organ or tissue	w_T	**LPA**	**UPA**	**RPO**	**LPO**	**LPOB**	**PAB**	**RPOB**	H_T (mSv)	I_T (%)	M_T (%)
Gonads	0.20	5.24	2.07	1.42	1.41	0.44	0.70	0.47	280	0.20	0.11
Red bone marrow	0.12	4.78	4.75	4.78	5.04	1.50	1.67	1.46	478	0.41	0.25
Colon	0.12	6.35	2.68	2.02	1.95	0.67	0.80	0.73	354	0.56	0.26
Lungs	0.12	4.51	7.86	4.24	4.34	1.72	2.10	1.75	553	2.79	2.45
Stomach	0.12	6.07	4.09	2.18	3.32	1.30	1.12	0.81	420	0.30	0.17
Bladder	0.05	4.06	1.67	1.32	1.37	0.44	0.55	0.45	228	0.35	0.10
Breasts	0.05	3.53	5.01	3.75	3.99	1.64	1.50	1.73	418	2.98	0.70
Liver	0.05	5.81	4.70	3.33	2.53	0.90	1.25	1.36	439	0.09	0.07
Esophagus	0.05	4.41	9.90	4.75	4.90	1.93	2.18	1.90	632		
Thyroid	0.05	2.22	8.18	7.45	7.79	2.89	2.74	2.95	619	1.70	
Skin	0.01	4.84	4.49	6.56	6.75	1.90	2.01	1.94	535	2.67	0.01
Bone surface	0.01	3.62	4.16	11.90	12.30	2.76	2.81	2.74	673		
Remainder	0.05	4.83	4.48	6.55	6.74	1.90	2.01	1.94	534	2.79	1.17
Boy Organ or tissue		H_T/D_{CTV} (mSv Gy^{-1})									
	w_T	LPA	UPA	RPO	LPO	LPOB	LLB		H_T (mSv)	I_T (%)	M_T (%)
Gonads	0.20	1.87	0.95	0.85	0.87	0.40	0.35		122		
Red bone marrow	0.12	2.33	1.67	1.44	1.51	0.59	0.41		179	0.22	0.13
Colon	0.12	7.88	2.73	1.54	1.80	0.70	0.58		391	0.94	0.46
Lungs	0.12	6.58	11.40	4.38	4.55	1.45	1.02		715	1.55	1.57
Stomach	0.12	8.31	4.92	2.12	3.06	0.89	0.82		504	0.28	0.15
Bladder	0.05	3.17	1.32	0.95	0.91	0.50	0.36		176	0.26	0.06
Breasts	0.05	4.92	5.96	4.18	4.31	1.10	1.04		488		
Liver	0.05	8.23	5.45	3.05	2.18	0.75	0.54		514	0.22	0.16

		H_T/D_{CTV} (mSv Gy^{-1})									
Girl Organ or tissue	w_T	**LPA**	**UPA**	**RPO**	**LPO**	**LPOB**	**PAB**	**RPOB**	H_T **(mSv)**	I_T **(%)**	M_T **(%)**
Esophagus	0.05	5.22	14.02	6.37	7.38	2.30	1.73		846		
Thyroid	0.05	2.37	13.79	9.78	10.94	3.51	2.67		884	0.44	
Skin	0.01	4.39	4.20	4.71	5.29	1.88	1.38		454	2.27	0.00
Bone surface	0.01	3.43	4.27	10.06	11.63	4.13	3.16		653		
Remainder	0.05	4.39	4.20	4.71	5.29	1.88	1.38		454	2.28	0.91

Abbreviations as in table 1.

Table 4

Summary of effective dose, E, predicted lifetime SMN incidence, I, and predicted lifetime SMN mortality, M, from neutrons. I_T and M_T are predicted lifetime SMN incidence and predicted lifetime SMN mortality, respectively, due to neutrons for specific cancer sites that correspond to organs and tissues, T.

Outcome	Girl	Boy
E (mSv)	428	418
I (%)	14.8	8.5
M (%)	5.3	3.4
Cancer sites with $I_T > 0.8\%$	Breast, lung, skin, thyroid	Skin, lung, colon
Cancer sites with $M_T > 0.4\%$	Lung, breast	Lung, colon